Chinese Chemical Letters 36 (2025) 110818

Contents lists available at ScienceDirect

Chinese Chemical Letters

journal homepage: www.elsevier.com/locate/cclet

Dual-functionality composites of polyaniline-coated oxidized carbon nanohorns: Efficient wave absorption and enhanced corrosion resistance

Haiyang Peng[a,b,c,1], Zhipeng Xie[a,b,c,1], Shuiqing Lu[a,b,c], Da Zhang[a,b,c,*], Bin Yang[a,b,c], Feng Liang[a,b,c,*]

[a] Faculty of Metallurgical and Energy Engineering, Kunming University of Science and Technology, Kunming 650093, China
[b] National Engineering Research Center of Vacuum Metallurgy, Kunming University of Science and Technology, Kunming 650093, China
[c] Key Laboratory for Nonferrous Vacuum Metallurgy of Yunnan Province, Kunming University of Science and Technology, Kunming 650093, China

ARTICLE INFO

Article history:
Received 15 October 2024
Revised 30 December 2024
Accepted 2 January 2025
Available online 3 January 2025

Keywords:
ox-CNHs@PANI
Core-shell structure
Electromagnetic wave absorption
Dielectric loss
Corrosion resistance

ABSTRACT

Electromagnetic wave-absorbing materials (EWAMs) are susceptible to failure in complex chemical environments. It is urgent to develop composites with high-efficiency electromagnetic wave (EMW) absorption and strong corrosion resistance. In the work, polyaniline (PANI) is *in-situ* polymerized on the surface of oxidized carbon nanohorns (ox-CNHs) to create a core-shell composite of ox-CNHs@PANI. By adjusting the thickness of the PANI shell and effectively regulating the electromagnetic parameters of the composite material, excellent impedance matching and efficient EMW absorption are achieved. At a thickness of 2.22 mm, the composite exhibits a reflection loss peak (RL_{min}) and a maximum effective absorption broadband (*EAB*) of −66.7 dB and 5.68 GHz, respectively. Additionally, the dense PANI shell effectively prevents contact between the corrosive medium and ox-CNHs, which significantly reduces the possibility of corrosion. Due to the formation of the ox-CNHs/PANI interface, the ox-CNHs@PANI composite exhibits strong corrosion resistance under acidic, alkaline, and neutral conditions. The ox-CNHs@PANI composite exhibits excellent EMW absorption and strong corrosion resistance, offering a new approach to developing advanced bifunctional materials.

Electromagnetic wave-absorbing materials (EWAMs) have garnered academic attention for mitigating the growing problem of electromagnetic pollution [1,2]. Over the past few decades, numerous EWAMs with high reflection loss and broad effective absorption bandwidths have been developed through the optimization of their composition and structure [3–5]. Among them, carbon nanohorns (CNHs) have attracted much attention for their large specific surface area, exceptional electrical conductivity, and the presence of abundant structural defects [6]. Additionally, CNHs are composed of aggregates with abundant horn-like structures, leading to the formation of numerous pores within the material [7]. These pore structures promote impedance matching and enhance dipole polarization [8]. Owing to these advantageous properties, CNHs are considered optimal candidates for EWAMs. However, the single-component CNHs are difficult to obtain satisfactory absorbing properties due to poor impedance matching. In order to solve this problem, a multi-component composite is an effective method. For example, ox-CNHs@SiO_2, F-CIP@CNHs, and Co@CNHs composites not only improved impedance matching but also enhanced electromagnetic wave (EMW) absorption performance through the synergistic effect between components [9–11].

Additionally, while satisfying the requirements for EMW absorption, pursuing multifunctionality can significantly expand the applications of EWAMs [12]. For instance, EWAMs are often exposed to complex chemical environments and lead to serious corrosion and reduce their EMW absorption properties [13,14]. To address the issue of poor corrosion resistance, an effective approach is to deposit or coat functional materials onto the surface of CNHs, forming a dense protective layer [15]. This protective layer acts as a barrier to block the infiltration of corrosive agents, thereby extending the service life of EWAMs. For example, NiAl-layered double hydroxide (NiAl-LDH) was deposited on graphene, and the risk of galvanic corrosion was alleviated by coating and protective passivation provided by the NiAl-LDH layer [16]. In addition, a multi-interface barrier structure is constructed by the maze effect, which

* Corresponding authors.
E-mail addresses: zhangda@kust.edu.cn (D. Zhang), liangfeng@kust.edu.cn (F. Liang).
[1] These authors contributed equally to this work.

https://doi.org/10.1016/j.cclet.2025.110818
1001-8417/

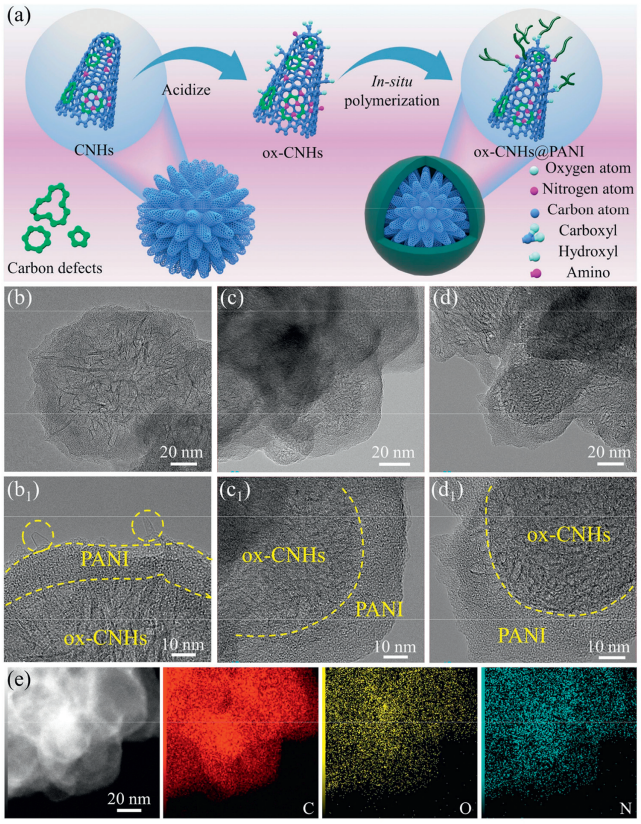

Fig. 1. (a) Schematic illustration of the synthesis process for the ox-CNHs@PANI composites. TEM images of (b, b_1) S0.25, (c, c_1) S0.5, and (d, d_1) S0.75. (e) EDS mapping of S0.5.

delays the corrosion process of the metal matrix [17]. Therefore, the development of composite materials with highly efficient EMW absorption and superior corrosion resistance is essential for the widespread application of EWAMs.

Herein, a novel core-shell structure is presented, wherein PANI is coated onto the surface of oxidized carbon nanohorns (ox-CNHs@PANI) *via in-situ* polymerization. The ox-CNHs@PANI demonstrates outstanding EMW absorption, with a reflection loss peak (RL_{min}) of −66.7 dB at a thickness of 2.22 mm and an effective absorption bandwidth (*EAB*) of 5.68 GHz. Furthermore, the composite demonstrates outstanding corrosion resistance in acidic, neutral, and alkaline environments. This study will open the possibility for the application and design of EWAMs suitable for complex chemical environments.

The fabrication process of ox-CNHs@PANI is shown in Fig. 1a. Firstly, active sites for the polymerization of aniline can be provided by acidification through oxygen-containing functional groups on the surface of CNHs [18]. Secondly, oxidative polymerization of aniline monomers is initiated by a water-soluble initiator in an acidic medium by the typical chemical oxidation method. To examine the influence of the PANI shell amount on the morphology of ox-CNHs@PANI, the samples are designated as S0.25, S0.5, and S0.75, corresponding to aniline volumes of 0.25, 0.5, and 0.75 mL, respectively.

The morphology of the ox-CNHs@PANI composites is investigated by transmission electron microscopy (TEM). Figs. 1b and b_1 show that the surface of ox-CNHs is coated with a thin layer of PANI, while some ox-CNHs remain exposed. As shown in Figs. 1c and c_1, ox-CNHs in S0.5 are completely enveloped by a thicker PANI layer. The PANI layer exhibited a distinct amorphous structure with clear demarcation from ox-CNHs. Figs. 1d and d_1 reveal a thicker PANI shell with an uneven thickness distribution. As shown in Fig. 1e, energy-dispersive spectroscopy (EDS) analysis of S0.5 indicates a uniform distribution of C, N, and O elements. Since the carbon content in PANI is lower than that of ox-CNHs, the carbon element distribution at the edge of the composite is relatively sparse.

As shown in Fig. 2a, XRD is used to characterize the phase structure of samples. All samples exhibit peaks at 26.4° and 42.2°, which are related to the graphitized structure, corresponding to (002) and (100) of graphite, respectively [19]. A shoulder peak located at nearly 26.4° is associated with the amorphous carbon structure. As the amount of PANI increases, the intensity of graphite diffraction peaks at near 26.4° and 42.2° gradually decrease. This reduction occurs because the X-rays experience more absorption and scattering when penetrating the shell layer [20]. The diffraction peaks of S0.5 and S0.75 broaden in the range of 20°−25° due to the higher content of amorphous PANI [21].

The molecular structures are further characterized through Fourier-transform infrared (FTIR) spectroscopy, as shown in Fig. 2b. The stretching vibrations of the C=N and C=O bonds at ∼1620 cm^{-1} and ∼1430 cm^{-1} are characteristic peaks of PANI [22,23]. The peaks at ∼1380 cm^{-1} and ∼1200 cm^{-1} correspond to the C-N stretching and C-N bending vibrations, respectively. The peak at ∼800 cm^{-1} corresponds to the bending vibration of the C–H bond on the aromatic ring [24]. The intensity of the absorption peak increases as the thickness of the shell layer increases.

The Raman spectra of ox-CNHs@PANI are shown in Fig. 2c, highlighting the spectral characteristics of different samples. The D band (around 1350 cm^{-1}) is associated with defects and disorder in the carbon material, while the G band (around 1580 cm^{-1}) corresponds to graphitized structure. Meanwhile, the I_D/I_G ratio is used to assess the level of defects in carbon materials [25]. In S0.25, the I_D/I_G ratio is 1.45. With the increase of PANI shell thickness, the I_D/I_G ratio increased to 1.44 at S0.5 and finally reached to 1.42 at S0.75. With the rise of PANI shell thickness, the degree of graphitization of the composites decreases. This indicates that the in-plane stretching vibration of sp^2 hybridized carbon atoms is enhanced, which contributes to improved absorption of EMW [26].

X-ray photoelectron spectroscopy (XPS) is employed to determine the detailed chemical states of ox-CNHs@PANI (Figs. 2d-g). The XPS survey spectra confirm that the samples primarily contained C, N, O, and S. In the C 1s spectrum, the peak at 284.8 eV corresponds to C-C and C=C bonds of graphitic carbon in CNHs [22]. The 285.54 eV peak is attributed to C-N bonds in PANI [27]. The peak at 289.37 eV is related to the C=O bond, which may originate from the ox-CNHs [22]. The N 1s spectrum can be deconvoluted into multiple peaks corresponding to different chemical environments in PANI: the peak at 399.6 eV for amine (-NH-), 401.3 eV for imines (-N=), and 406.2 eV for protonated nitrogen ($-N^+$) [28]. The O 1s spectrum shows major peaks for oxygen-containing groups: 533.2 eV for hydroxyl groups (-OH), 532.4 eV for carbonyl or carboxyl groups (C=O), and 530.6 eV for ether bonds (C-O-C) [29]. C-O-C is formed by the oxidation of C in the PANI unit to form hydroxyl groups, and the hydroxyl groups continue to be oxidized [30]. Together, ox-CNHs@PANI composites are successfully synthesized based on these results.

The conductivity of ox-CNHs@PANI gradually increases with the thickness of the PANI shell, as shown in Fig. 2h. It is worth noting that the conductivity of S0.75 is significantly enhanced compared to S0.5. The local accumulation of PANI can be connected to form a conductive network, which significantly improves the conductivity. In addition, as shown in Fig. 2i, as the shell thickness increases, the bulk density increases slightly. Since the density of polyaniline is higher than that of CNHs, although the bulk density increases

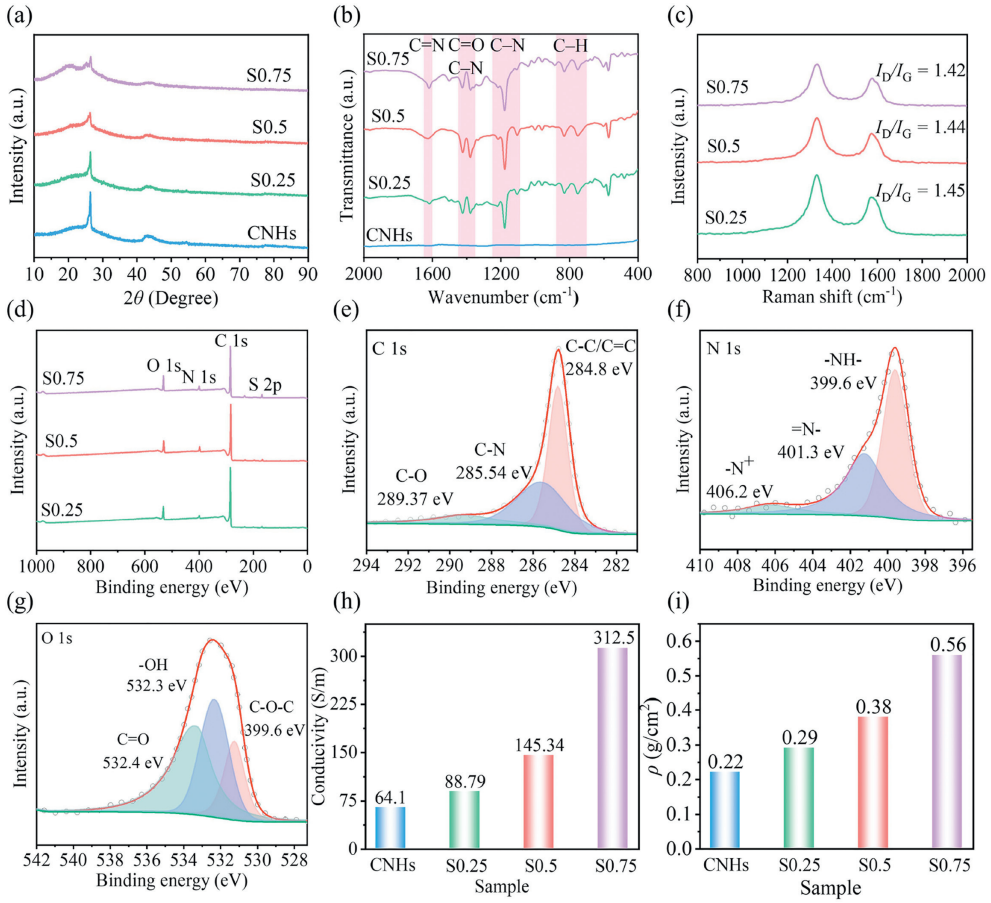

Fig. 2. Characterization of CNHs, S0.25, S0.5, and S0.75. (a) XRD patterns, (b) FTIR spectra, (c) Raman spectra, (d-g) XPS spectra, (h) conductivity, (i) bulk density.

slightly after coating, the material remains an excellent lightweight EWAMs.

To elucidate the mechanism underlying EMW absorption performance, the electromagnetic parameters are preliminarily analyzed. According to the free electron theory ($\varepsilon'' \approx \sigma/2\sigma_0 f$), the values of ε'' are positively correlated with the conductivity (σ) [31]. The ε' of ox-CNHs@PANI exhibits pronounced dispersion, while the ε'' displays continuous resonance peaks at medium and high frequencies (Figs. 3a and b) [32]. The polarization ability and dielectric loss are enhanced by the introduction of PANI (Fig. S2c in Supporting information). The α values increased with increasing frequency and decreased the PANI content (Fig. 3c). It is worth noting that the imaginary parts of the complex permeability of CNHs and S0.75 are partly negative at high frequencies. The increase of conductivity leads to the formation of an induced electric field within the material, consequently generating a new induced magnetic field that radiates electromagnetic energy outward (Fig. S2 in Supporting information) [33].

Cole-Cole plots illustrate the relationship between ε' and ε'', with each semicircle corresponding to a single Debye relaxation process (Figs. 3d-g) [34,35]. All samples show multiple semicircles at low frequencies, corresponding to multiple polarization reactions [36]. For ox-CNHs@PANI, dipole polarization is caused by defects in the CNHs and the uneven charge distribution at the oxygen-containing functional groups. Meanwhile, interfacial polarization is induced by electron accumulation at the ox-CNHs/PANI heterogeneous interface [37]. In addition to the polarization reaction, a straight line appears at the end of the Cole-Cole curve, indicating the existence of conductivity loss. Compared with CNHs, the conductivity loss of ox-CNHs@PANI is significantly enhanced. To analyze the contributions of polarization loss and conduction loss to dielectric loss, a parallel/series circuit model of resistance and capacitance is used. Combined with nonlinear least-squares fitting, the dielectric loss is then decomposed (Figs. 3h and i) [38]. The results indicate that dielectric loss is primarily due to conduction loss.

To examine the influence of PANI shell thickness on the absorption properties of the composites, the *RL* values of ox-CNHs@PANI are analyzed based on transmission line theory. According to Eq. S6 (Supporting information), to achieve optimal impedance matching, it is essential for Z_{in} to closely approximate Z_0. When $Z_{in}/Z_0 = 1$, EWAMs achieve perfect impedance matching to ensure that as many EMW as possible enter the material [39]. Fig. 4 and Fig. S2 illustrate the loss characteristics of S0.25, S0.5, and S0.75 at different thicknesses. S0.25 consistently shows an impedance matching condition above 1.2 across all thicknesses (Figs. 4a and a_1). S0.5 maintains an impedance matching ranging from 0.8 to 1.2 across different thicknesses. Besides, it is indicated that most of the thickness is less than 1 in S0.75. (Figs. 4c and c_1). S0.5 exhibits excellent EMW absorption performance due to effective combination of attenuation constant and impedance matching. At a thickness of 2.22 mm, the RL_{min} reaches to −66.7 dB, whereas an *EAB* of 5.68 GHz is obtained (Figs. 4b and b_1). The loss capacity of S0.25 is low, resulting in poor loss capacity. With the increase of PANI content, the skin effect of S0.75 becomes more significant. This means that EMW can only penetrate the surface layer of the material, limiting its effective attenuation.

Radar cross-section (RCS) simulations using CST Studio software further demonstrate invisible properties of the composites [40]. As shown in Figs. 5a-d and Fig. S3 (Supporting information), com-

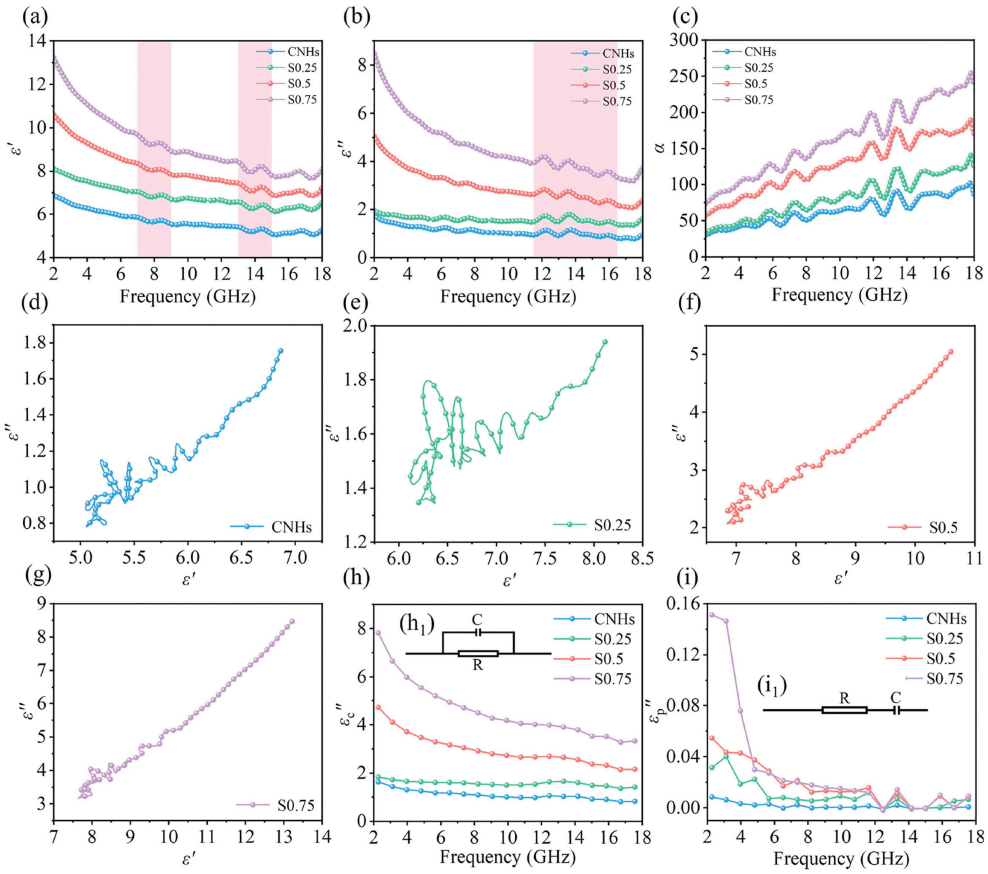

Fig. 3. The dielectric properties of CNHs, S0.25, S0.5, and S0.75. (a, b) ε' and ε'', respectively. (c) α, (d-g) Cole-Cole semicircles, (h, i) conduction loss and polarization loss, respectively, (h_1, i_1) equivalent parallel and series circuits, respectively.

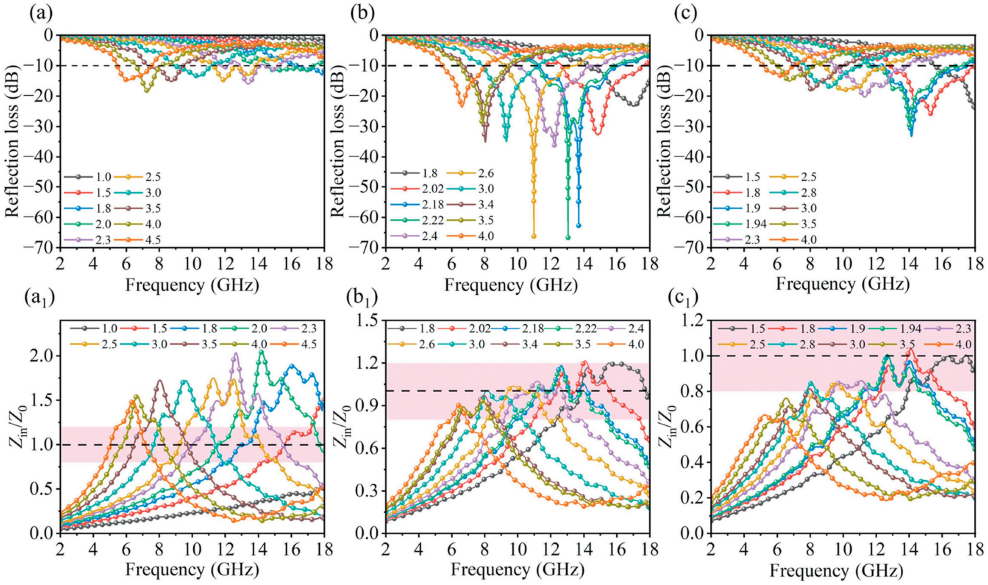

Fig. 4. *RL* curves and impedance matching curves of (a, a_1) S0.25, (b, b_1) S0.5, and (c, c_1) S0.75.

pared to the ideal electrical conductor (PEC), ox-CNHs@PANI effectively reduce the RCS. Among them, the RCS of S0.5 remains below −20 dB m² at most angles of incidence ($-90° \leq \varphi \leq 90°$). It shows that S0.5 is expected to be an excellent EMW stealth material in practical applications. The minimum RCS values of PEC coated by S0.25, S0.5, and S0.75 are −49.8, −50.08, and −27.6 dB m^2, respectively, significantly lower than that of PEC (−21.7 dB m^2). In comparison with the typical carbon-based EWAMs in Fig. 5e, ox-CNHs@PANI demonstrates the wide *EAB* of 5.58 GHz and strong absorption of −66.67 dB.

Through the above analysis, the possible EMW absorption mechanism of the composite material is shown in Fig. 5f. Firstly, ox-CNHs and PANI provide a conductive path for the transmission of electrons in the material, thereby increasing the conductive

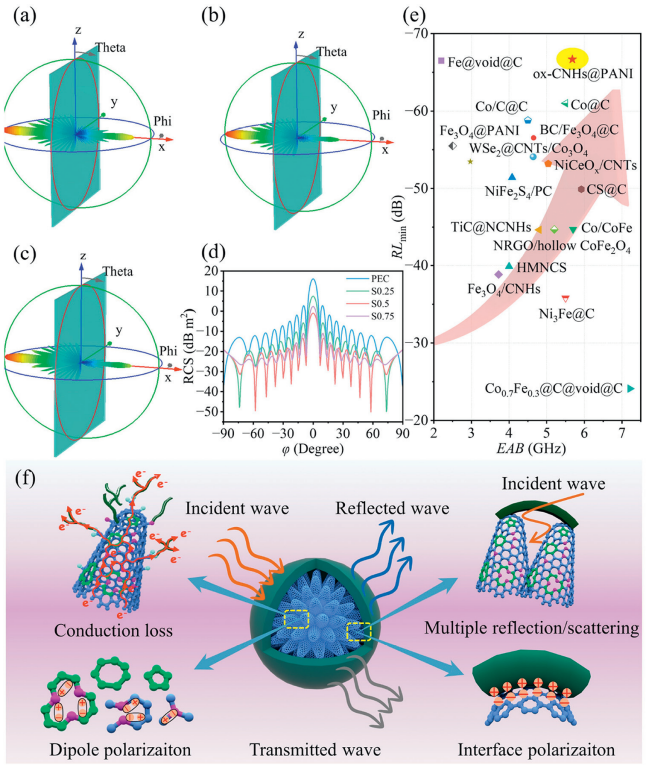

Fig. 5. The 3D RCS values of (a) S0.25, (b) S0.5, (c) S0.75, (d) 2D RCS values. (e) Comparison of RL_{min} and *EAB* between the ox-CNHs@PANI and typical carbon-based EWAMs. (f) Schematic illustration of EMW absorption mechanism for ox-CNHs@PANI.

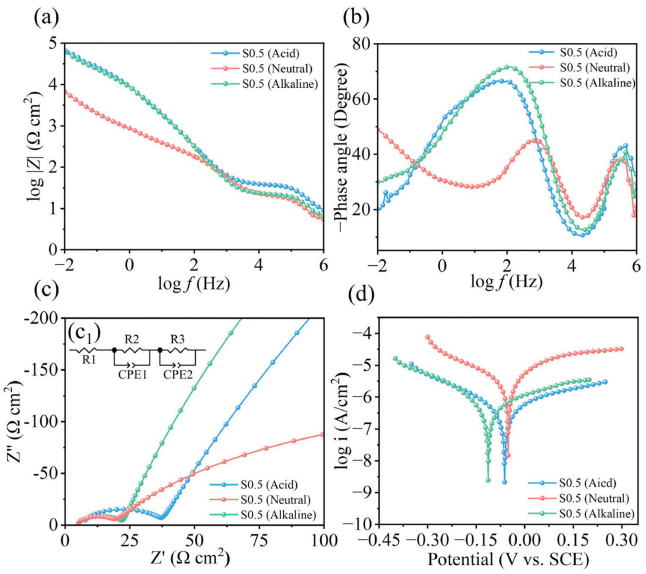

Fig. 6. Electrochemical characterization of S0.5 in acidic, alkaline, and neutral conditions. (a) impedance-frequency bode plot, (b) phase-frequency bode plot, (c) Nyquist chart, (c_1) equivalent circuit, (d) Tafel plot.

Table 1
Corrosion kinetic parameters of S0.5 immersed in acidic, neutral, and alkaline solutions, respectively.

Solution	E_{corr} (V)	I_{corr} (A/cm^2)	β_a (mV)	β_c (mV)	R_p (Ω)
Acidity	−0.062	4.242×10^{-7}	6.019	4.472	97,689.9
Neutral	−0.051	3.907×10^{-6}	5.074	5.580	10,519.0
Alkaline	−0.113	5.048×10^{-7}	7.057	4.229	76,318.0

loss of the material [41]. Secondly, the "dahlia-like" ox-CNHs create more internal space, enhancing the multiple scattering and reflection of EMW. Additionally, due to differences in conductivity and resistance, a large number of space charges redistribute and accumulate at the heterogeneous interface between ox-CNHs and PANI, which enhances the interface polarization effect [42]. The synergy of the aforementioned dielectric loss mechanisms enables the ox-CNHs@PANI to efficiently attenuate incident EMW energy (Fig. 5f and Fig. S2).

To study the corrosion resistance based on excellent EMW absorbing performance, this paper focuses on S0.5 and investigates its corrosion resistance in 3.5 wt% NaCl solution, sodium hydroxide solution (pH 13.6), and hydrochloric acid solution (pH 1.3). Electrochemical impedance spectroscopy (EIS) and Tafel curves are carried out (Fig. S4 in Supporting information). Impedance-frequency Bode diagram illustrates the trend of impedance modulus variation with frequency, allowing for a visual representation of the impedance characteristics [30]. At 0.01 Hz, the impedance modulus serves as a semi-quantitative measure of coating impedance [43]. Within the frequency range of 0.01–100 Hz, S0.5 has significantly higher impedance in acidic and alkaline solutions compared to neutral solutions, as shown in Fig. 6a. This indicates that it had better corrosion resistance in these environments. High-frequency phase angles also serve as effective parameters for evaluating coating protection. Fig. 6b reveals the higher coating resistance results in a larger phase angle between current and voltage. S0.5 shows large phase angles, indicating that the samples have effective capacitive properties that act as a barrier to corrosive media [44]. Fig. 6c shows the EIS data of the S0.5 under acidic, alkaline, and neutral conditions. The larger the radius of the corresponding charge-transfer resistance, the stronger the charge-transfer resistance ability of the sample. The above results show that ox-CNHs@PANI exhibits large impedance in acidic, neutral, and alkaline solutions, which effectively hinders the charge exchange between Cl^-, H^+, OH^-, and the ox-CNHs@PANI.

The Tafel plot shows corrosion potential (E_{corr}) and corrosion current (I_{corr}) are used to assess the stability of coatings [45]. Generally, positive E_{corr} and lower I_{corr} reflect better corrosion resistance. Fig. 6d displays Tafel curves for samples after about 1 h in different solutions, with corresponding data in Table 1 and Table S1 (Supporting information). The corrosion potential of ox-CNHs@PANI is positively shifted compared to that of ox-CNHs, which indicates a reduced tendency to self-corrosion [46]. S0.5 shows excellent corrosion resistance in all environments, especially in acidic conditions with I_{corr} as low as 4.242×10^{-7} A/cm^2.

The corrosion resistance of ox-CNHs@PANI is due to the dense PANI shell on ox-CNHs. This shell effectively prevents corrosive substances such as moisture, oxygen, and ions from entering ox-CNHs. In addition, PANI delays the onset of corrosion by providing electrons through redox reactions that counteract electron loss [47]. Therefore, ox-CNHs@PANI exhibits excellent corrosion resistance and stability under three conditions.

In summary, ox-CNHs@PANI composites with the core-shell structure are successfully synthesized by *in-situ* polymerization. Those composites have excellent EMW absorption properties thanks to thoughtful component design and multi-interface synergies. The ox-CNHs@PANI composite exhibits excellent EMW absorption performance at both thin thicknesses and low filling amounts. When the thickness of the composite is 2.22 mm, the RL_{min} and EAB can reach to −66.7 dB and 5.68 GHz with a filler content of 25 wt%, respectively. In addition, the ox-CNHs@PANI composite has excellent corrosion resistance and is used in the variety of complex environment. This work can inspire the further development of functional EWAMs tailored to meet the specific requirements of corrosion resistance.

Declaration of competing interest

The authors declare that they have no known competing financial interests or personal relationships that could have appeared to influence the work reported in this paper.

CRediT authorship contribution statement

Haiyang Peng: Writing – original draft, Visualization, Investigation, Conceptualization. **Zhipeng Xie:** Visualization, Methodology, Conceptualization. **Shuiqing Lu:** Software, Methodology. **Da Zhang:** Writing – review & editing, Formal analysis. **Bin Yang:** Investigation. **Feng Liang:** Writing – review & editing, Funding acquisition.

Acknowledgments

The work was financially supported by the National Natural Science Foundation of China (Nos. 12175089, 12205127, 52220105010), the Key Research and Development Program of Yunnan Province (No. 202103AF140006), the Applied Basic Research Programs of Yunnan Provincial Science and Technology Department (Nos. 202001AW070004, 202301AS070051, 202301AU070064), Yunnan Industrial Innovative Talents Program for "Xingdian Talent Support Plan" (No. KKXY202252001), Yunnan Program for Introducing Foreign Talents (No. 202305AO350042), and Yunnan Major Scientific and Technological Projects (No. 202202AG050003).

Supplementary materials

Supplementary material associated with this article can be found, in the online version, at doi:10.1016/j.cclet.2025.110818.

References

[1] P. Liu, S. Zheng, Z. He, et al., Small 20 (2024) 2403903.
[2] R. Shu, Z. Zhao, X. Yang, Chem. Eng. J. 473 (2023) 145224.
[3] H. Fu, Y. Guo, J. Yu, et al., Chin. Chem. Lett. 33 (2022) 957–962.
[4] R. Shu, K. Yun, X. Liu, L. Xu, Compos. Part A 188 (2025) 108558.
[5] R. Shu, L. Nie, Z. Zhao, X. Yang, J. Mater. Sci. Technol. 175 (2024) 115–124.
[6] N. Karousis, I. Suarez-Martinez, C.P. Ewels, N. Tagmatarchis, Chem. Rev. 116 (2016) 4850–4883.
[7] J. Xu, H. Tomimoto, T. Nakayama, Carbon 49 (2011) 2074–2078.
[8] P. Liu, S. Gao, X. Liu, et al., Compos. Part B: Eng. 192 (2020) 107992.
[9] Z. Xie, Y. Liu, S. Lu, et al., Chem. Eng. J. 489 (2024) 151311.
[10] S. Lu, Z. Xie, D. Zhang, et al., Carbon 230 (2024) 119632.
[11] Z. Zhang, Y. Nan, J. Wei, Y. Zhou, M. Qiao, J. Alloys Compd. 922 (2022) 166201.
[12] P. Liu, S. Gao, Y. Wang, et al., Compos. Part B: Eng. 202 (2020) 108406.
[13] Z. He, L. Shi, R. Sun, et al., Nano-Micro Lett. 17 (2025) 1–14.
[14] W. Tian, X. Zhang, Y. Guo, et al., Carbon 173 (2021) 185–193.
[15] J. Zhou, Y. Liu, C. Zhou, et al., Chem. Eng. J. 477 (2023) 147042.
[16] X. Xu, S. Shi, Y. Tang, et al., Adv. Sci. 8 (2021) 2002658.
[17] J. Zhou, Y. Liu, C. Zhou, et al., Chem. Eng. J. 477 (2023) 147042.
[18] Y. Wang, X. Gao, Y. Fu, et al., Compos. Part B: Eng. 169 (2019) 221–228.
[19] L. Deng, R. Shu, J. Zhang, J. Colloid Interface Sci. 614 (2022) 110–119.
[20] P. He, W. Ma, J. Xu, et al., Small 19 (2023) 2302961.
[21] F. Zhang, W. Cui, B. Wang, et al., Compos. Part B: Eng. 204 (2021) 108491.
[22] L. Liang, Z. Li, Z. Bai, et al., Chin. Chem. Lett. 32 (2021) 870–874.
[23] D. Lan, Y. Wang, Y. Wang, et al., Colloid Interface Sci. 651 (2023) 494–503.
[24] M. Yu, Y. Huang, X. Liu, et al., Carbon 208 (2023) 311–321.
[25] L. Yuan, W. Zhao, Y. Miao, et al., Adv. Compos. Hybrid Mater. 7 (2024) 70.
[26] Y. Wu, K. Peng, Z. Man, et al., Carbon 188 (2022) 503–512.
[27] Z. Zhang, G. Zhang, L. Lei, et al., Ceram. Int. 48 (2022) 18338–18347.
[28] S. Kang, S. Qiao, Z. Hu, et al., J. Mater. Sci. 54 (2019) 6410–6424.
[29] Y. Liu, Z. Xie, S. Lu, et al., Dalton Trans. 53 (2024) 11454–11463.
[30] J. Liu, Y. Gu, L. Gao, et al., Appl. Surf. Sci. 613 (2023) 156098.
[31] Y. Wang, R. Cheng, W. Cui, et al., Carbon 210 (2023) 118043.
[32] L. Meng, J. Wang, J. Qi, et al., J. Colloid Interface Sci. 659 (2024) 945–958.
[33] T. Gao, R. Zhao, Y. Li, et al., Adv. Funct. Mater. 32 (2022) 2204370.
[34] J. Hu, Y. Hu, Y. Ye, R. Shen, Chem. Eng. J. 452 (2023) 139147.
[35] R. Peymanfar, A. Mirkhan, Chem. Eng. J. 446 (2022) 136903.
[36] X. Lin, Y. Zhou, J. Hong, et al., Chin. Chem. Lett. 35 (2024) 109835.
[37] X. Liu, J. Zhou, Y. Xue, X. Lu, Nano-Micro Lett. 16 (2024) 174.
[38] Y. Guo, J. Su, T. Bian, et al., Phys. Chem. Chem. Phys. 25 (2023) 8244–8262.
[39] J. Wang, L. Zhang, J. Yan, et al., Adv. Funct. Mater. 34 (2024) 2402419.
[40] G. Shao, X. Shen, X. Huang, ACS Mater. Lett. 4 (2022) 1787–1797.
[41] R. Shu, L. Xu, Y. Guan, J. Colloid Interface Sci. 675 (2024) 401–410.
[42] R. Shu, Y. Guan, B. Liu, J. Mater. Sci. Technol. 214 (2025) 16–26.
[43] Z. Zhang, J. Tan, W. Gu, et al., Chem. Eng. J. 395 (2020) 125190.
[44] H. Zhou, L. Jiang, L. Jia, et al., Alloy Compd. 959 (2023) 170579.
[45] J. Yang, Z. Liu, H. Zhou, et al., ACS Appl. Mater. Inter. 14 (2022) 12375–12384.
[46] J. Li, M. Huang, W. Gao, K. Yao, H. Ma, ACS Appl. Polym. Mater. 6 (2024) 5662–5673.
[47] Z. Zhang, J. Yuan, G. Lian, et al., J. Alloy Compd. 988 (2024) 174175.